doi:10.1016/j.jmb.2005.09.075 J. Mol. Biol. (2005) 354, 473–482

JMB

Available online at www.sciencedirect.com

SCIENCE DIRECT®

ELSEVIER

# A Single Disulfide Bond Differentiates Aggregation Pathways of ß2-Microglobulin

**Yiwen Chen[1] and Nikolay V. Dokholyan[2]***

[1]*Department of Physics and Astronomy, University of North Carolina at Chapel Hill, Chapel Hill, NC 27599, USA*

[2]*Department of Biochemistry and Biophysics, University of North Carolina at Chapel Hill Chapel Hill, NC 27599, USA*

**Corresponding author*

Deposition of wild-type ß2-microglobulin (ß2m) into amyloid fibrils is a complication in patients undergoing long-term hemodialysis. The native ß-sandwich fold of ß2m has a highly conserved disulfide bond linking Cys25 and Cys80. Oxidized ß2m forms needle-like amyloid fibrils at pH 2.5 *in vitro*, whereas reduced ß2m, at acid pH, in which the intra-chain disulfide bond is disrupted, cannot form typical fibrils. Instead, reduced ß2m forms thinner and more flexible filaments. To uncover the difference in molecular mechanisms underlying the aggregation of the oxidized and reduced ß2m, we performed molecular dynamics simulations of ß2m oligomerization under oxidized and reduced conditions. We show that, consistent with experimental observations, the oxidized ß2m forms domain-swapped dimer, in which the two proteins exchange their N-terminal segments complementing each other. In contrast, both dimers and trimers, formed by reduced ß2m, are comprised of parallel ß-sheets between monomers and stabilized by the hydrogen bond network along the backbone. The oligomerized monomers are in extended conformations, capable of further aggregation. We find that both reduced and oxidized dimers are thermodynamically less stable than their corresponding monomers, indicating that ß2m oligomerization is not accompanied by the formation of a thermodynamically stable dimer. Our studies suggest that the different aggregation pathways of oxidized and reduced ß2m are dictated by the formation of distinct precursor oligomeric species that are modulated by Cys25-Cys80 disulfide-bonds. We propose that the propagation of domain swapping is the aggregation mechanism for the oxidized ß2m, while "parallel stacking" of partially unfolded ß2m is the aggregation mechanism for the reduced ß2m.



*Keywords:* ß2-microglobulin; dialysis-related amyloidosis (DRA); disulfide bond; molecular dynamics simulation; aggregation; domain swapping

## Introduction

Amyloid fibrils are insoluble aggregates of peptides or usually soluble proteins.[1–3] Electron microscopy[4] and X-ray diffraction[5,6] studies have established that the amyloid fibrils are straight, long and unbranching filaments with a high content of ß-sheets. Amyloid fibrils are typically 70–120 Å in diameter, and several thousand angstroms in length. A wide variety of proteins and peptides can self-assemble into amyloid fibrils with a common cross-ß structure despite a large variation in their sequences and native structures, suggesting a common mechanism underlying amyloid fibril formation. The deposition of proteins into amyloid fibrils is associated with many human diseases, such as Aβ in Alzheimer's disease,[7,8] prion in transmissible spongiform encephalopathy,[9] and ß2-microglobulin (ß2m) in dialysis-related amyloidosis.[10,11] Dialysis-related amyloidosis involves deposition of ß2m amyloid typically in collagen-rich tissues, such as cartilage,[12] resulting in carpel tunnel syndrome and pathological bone destruction. Deposition of ß2m amyloid is a serious complication in patients receiving hemodialysis for more than ten years.[13]

Abbreviations used: ß2m, ß2-microglobulin; DRA, dialysis-related amyloidosis; MHC-I, major histocompatibility complex class I; DMD, discrete molecular dynamics; MM-PB/SA, molecular mechanics-Poisson Boltzmann/surface area.

E-mail address of the corresponding author: dokh@med.unc.edu

ß2m, the light-chain of the antigen class I major histocompatibility complex (MHC-I), is localized on the cell surface. ß2m is necessary for the cell-surface expression of MHC-I. During its normal catabolic cycle, ß2m dissociates from the MHC-I complex and is transported in the serum to the kidneys where the majority is degraded.[11] Renal failure interferes with normal clearance of ß2m in serum, resulting in an increase in concentration of ß2m in serum.[11] Through an undetermined mechanism, ß2m then forms amyloid fibrils that typically accumulate in the musculoskeletal system.[12]

ß2m is a 99 residue protein with a molecular mass of 11.8 kDa that belongs to the immunoglobin superfamily and has a seven-stranded ß-sandwich fold.[14,15] The two ß-sheets (one consisting of ß-strands A,B,D,E and the other ß-strands C, F, G; Figure 1(a) and (b)) are connected by a single disulfide bond linking Cys25 and Cys80 in ß-strands B and F (Figure 1(c)). This disulfide bond is highly conserved in the immunoglobin superfamily and stabilizes the native fold of these proteins.[16,17] *In vitro* oxidized ß2m is stable at neutral pH, so that the formation of amyloid fibrils requires significant destabilization, which can be achieved *via* deletions of N-terminal six residues,[18] mutations at terminal ß-strands,[19] addition of $Cu^{2+}$,[20] addition of pre-formed aggregation-nucleating seeds,[21] and by concentrating and drying the protein on a dialysis membrane surface.[22] At acidic pH, oxidized ß2m can rapidly form fibrils with a range of different morphologies.[23–26] The fibrils produced by incubation of oxidized ß2m at pH 3.6 are short (<600 nm) and have curvilinear morphology, while those produced by incubation of oxidized ß2m at pH 2.5 are long (~1 μm) and straight.[25,27] The latter amyloid fibril morphology is typical for aggregates accumulated in patients' tissues. In contrast, at a wide range of acidic pH from pH 4.0 to pH 1.5, when the disulfide bond is disrupted, ß2m does not form typical amyloid fibrils like those observed in patients' tissues. Instead, reduced ß2m forms thin and flexible filaments,[26–28] suggesting a different molecular mechanism for aggregation of reduced *versus* oxidized ß2m. The molecular mechanisms leading to distinct aggregation pathways and morphologies of oxidized *versus* reduced ß2m are largely unknown.

There is increasing evidence that assembly of the partially unfolded state of proteins into non-fibrillar oligomeric species[29–35] precedes nucleation-dependent fibril formation.[32,33,36–38] This suggests that structural properties of precursor oligomeric species may differentiate the morphologies of amyloid fibrils obtained under various experimental conditions. Therefore, understanding the differences in structure and aggregation mechanisms of early oligomers of oxidized and reduced ß2m may offer insights into large-scale morphological properties of ß2m aggregates.

Experimental structural and kinetic studies of the oligomeric ß2m states are challenging because these states are often short-lived. Computational approaches have been pivotal in offering experimentally testable hypotheses that aid in elucidating the structure and formation mechanism of oligomeric intermediates.[39–42] All-atom molecular dynamics simulations have offered important insights into the partially unfolded states of the precursor proteins or peptides under acidic or high temperature conditions and the aggregation of small peptides.[41,43–46] However, all-atom molecular dynamics simulations have severe limitations on the time and length scales that are accessible. Discrete molecular dynamics (DMD)[47] simulations of simplified protein models have extended the "visible" time and length scales in a number of studies.[39,42,48,49] Here we capitalize on this strength of DMD[50–52] to study oligomerization of the reduced and oxidized ß2m.

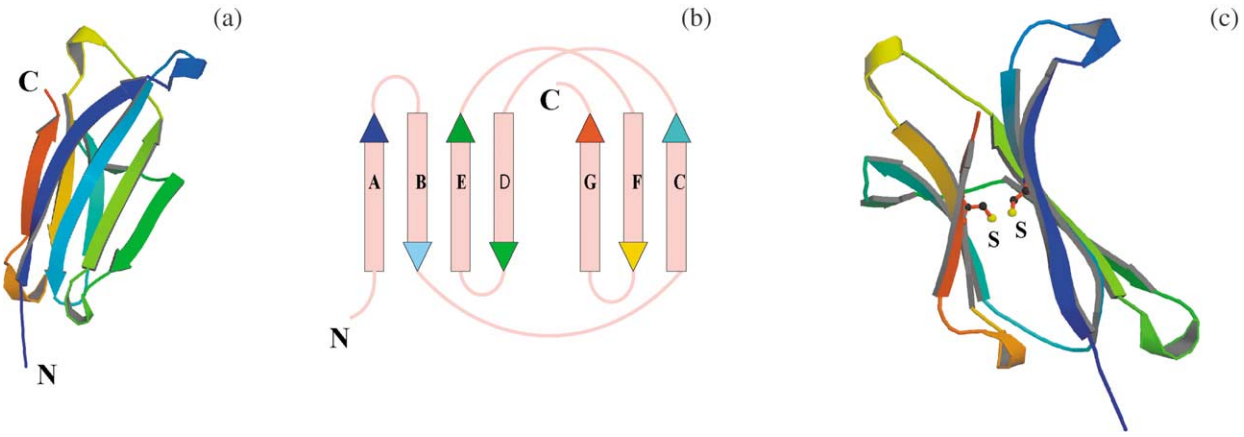


**Figure 1.** Schematic representation of the native fold of ß2m: (a) the native structure of ß2m; (b) the connection diagram of seven β-strands from N to C terminus; (c) the disulfide bond between Cys25 and Cys80. Starting from the N terminus, the seven β-strands are named sequentially A, B, C, D, E, F, and G. There are two β-sheets connected by the disulfide bond between Cys25 and Cys80. One β-sheet is formed by strands A (blue), B (light blue), D (light green), E (green) and the other one is formed by strands C (cyan), F (gold), G (red). All structures are produced using Molscript[88] and Raster3D.[89]

## Results

### Oligomerization of the reduced ß2m

It has been shown that protein oligomerization occurs under destabilizing conditions, for example by increasing a system's temperature to folding transition temperature $T_f$.[39] Therefore, we study heat denaturation of reduced ß2m to determine $T_f$. We perform DMD simulations of ß2m using the Gō[53,54] potential assigned based on the X-ray crystal structure of ß2m (Materials and Methods). We perform equilibrium simulations at various system temperatures ranging from $T=0.1$ to $T=2.0$ (simulation temperature is in the units of $\epsilon/k_B$, where $\epsilon$ is the interaction energy unit and $k_B$ is the Boltzmann's constant). The temperature dependencies of the potential energy and the root-mean-square deviation (RMSD) from the native state of reduced ß2m are shown in Figure 2. The midpoint of the sigmoidal increase in potential energy and RMSD as a function of temperature corresponds to $T_f$.[50] At low temperatures, ß2m exists mostly in the folded state as signified by small RMSD from the native structure ($<3$ Å) and low average potential energy. At high temperatures, ß2m exists mostly in unfolded conformations with large RMSD ($>29$ Å), indicating significant loss of structural similarity to the native structure.

Next, we perform equilibrium simulations of two copies of reduced ß2m at various temperatures ranging from 0.1 to 2.0. Folding and dimerization are two competing processes.[3] We observe dimer formation at temperatures between two threshold temperatures $T_M \approx 0.77$ and $T_D \approx 1.00$. At temperatures below $T_M$, where the free energy folding barrier of each monomer is lower than that of dimer formation, two ß2m fold separately without dimerization. At temperatures between $T_M$ and $T_D$, where the free energy barrier of dimer formation is lower than that of folding, ß2m dimerization is dominant. At temperatures above $T_D$, two monomers both predominantly exist in unfolded states.

Experimental studies suggest that the arrangement of ß strands in amyloid fibrils can be either parallel or antiparallel. For example, amyloid fibrils formed by residues 34–42 of Aβ(1-42) were determined to adopt an antiparallel configuration by FTIR spectroscopy[55] and solid-state NMR spectroscopy.[56] In contrast, Benzinger *et al.*[57] showed by solid-state NMR that the Aβ(10-35) fibril adopts a parallel β-sheet structure. We find that the reduced ß2m dimer adopts a parallel ß-sheet structure formed by monomers in extended conformations (Figure 3). The native ß-sandwich fold is significantly unfolded in the reduced ß2m dimer. The inter-sheet contacts connecting two ß-sheets (consisting of ß-strands A, B, D, E and the other ß-strands C, F, G) in the native structure are mostly disrupted in the dimer structure and the hydrophobic core is exposed. The formation of intermolecular hydrogen bonds along ß2m backbones stabilizes the parallel ß-strands structure between monomers.

To investigate the formation of higher-order oligomers, we perform DMD simulations with three reduced ß2m chains following the same simulation protocol as in the dimer simulations. We observe that the reduced ß2m trimer adopts an overall similar structure to the dimer (Figure 4(a)). The monomers are significantly unfolded in extended conformations, stacked in parallel to each other, and form an inter-chain ß-sheet structure. The loss of intra-molecular native interactions is compensated by the formation of inter-molecular and hydrogen bond interactions along the backbones between monomers. The remarkable similarity between trimer and dimer structures suggests that the elongation of oligomers from

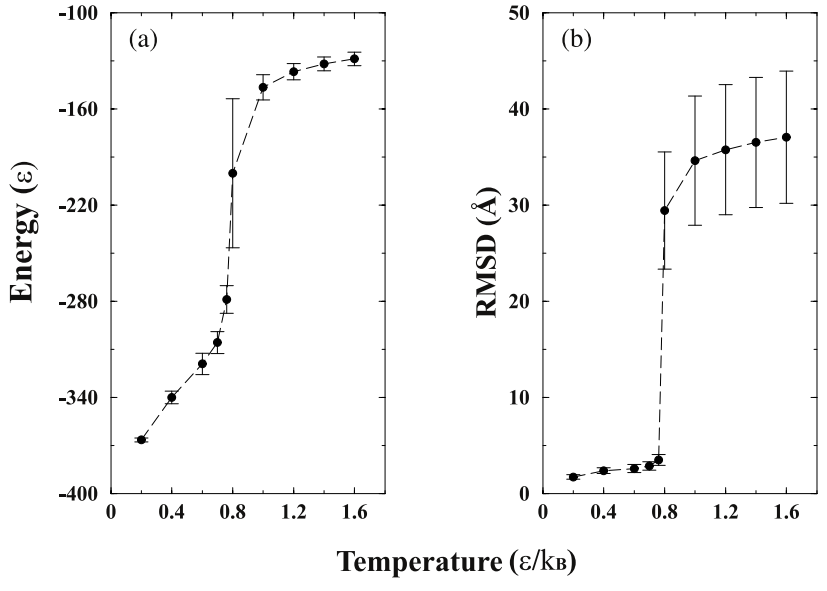


**Figure 2.** Heat denaturation curve of the reduced ß2m. The dependence on temperature of (a) the potential energy (in the interaction energy units $\epsilon$) and (b) the RMSD from the native structure. The folding transition temperature, which is at the midpoint of the heat denaturation curve, is approximately $T_f \approx 0.80$ (in the units of $\epsilon/k_B$).

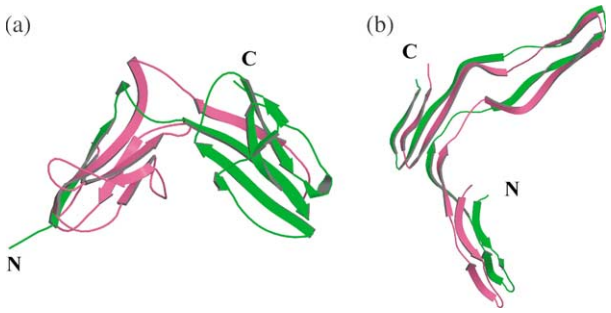


**Figure 3.** The structures of dimers formed by (a) oxidized and (b) reduced ß2m. The structures represent typical snapshots from DMD simulation trajectories near $T_f$. Two monomers in a dimer are represented using pink and green colors. The oxidized ß2m forms a domain swapped structure, while the reduced ß2m forms a parallel β-structure between monomers with extended conformations.

$n$-mer to $(n+1)$-mer proceeds through the same mechanism as from dimer to trimer. When the $(n+1)^{th}$ monomer interacts with the $n$-mer, it tends to adopt a similar extended structure to the monomer structure in $n$-mer, so that the number of backbone hydrogen-bond formations is maximized. We further build a structural model of early aggregate for reduced ß2m in this "parallel stacking" scenario (Figure 4(b)). Due to the limit of computational power, we develop and use a DMD-aided docking methodology starting from a pre-defined, rather than random, configuration (Materials and Methods) to bring together five trimers to form 15-mers by taking into account the flexibility of molecules without disrupting the overall topology of each trimer.

## Oligomerization of the oxidized ß2m

The oxidized ß2m has a similar heat denaturation curve to that of the reduced form (data not shown), except for the $T_f$, which is approximately 0.97 for oxidized ß2m and is approximately 0.80 for reduced ß2m (Figure 2). The lower $T_f$ of the reduced ß2m compared with the oxidized form indicates that the loss of disulfide bond destabilizes the native state and is consistent with the experimental findings.[26]

To study the formation of dimer, we perform equilibrium simulations of two copies of the oxidized ß2m at various temperatures ranging from 0.1 to 2.0. We observe dimer formation in simulations at temperatures between two threshold temperatures $T_M \approx 0.97$ and $T_D \approx 1.10$. Below $T_M$ we observe that two ß2m monomers fold separately without dimerization. Above $T_D$ we find that ß2m monomers are both in unfolded states. Ordered dimer formation only occurs below $T \approx 1.04$. In contrast to the extended dimer structures observed in the simulation of reduced ß2m, we observe formation of domain-swapped ß2m dimers, in which the two proteins exchange their N-terminal segment complementing each other[39,58] (Figure 3). Thus, most of the native fold and overall compactness remain in this dimer structure.

There are approximately 40 structurally characterized cases of domain-swapped proteins,[58] including human prion,[59] RNase A[60,61] and staphylococcal nuclease.[62] The evidence of domain swapping as a mechanism of amyloid fibril formation has been observed in cystatin C[63] and prion protein.[59] In addition, domain swapping has been proposed as a possible mechanism for the ß2m amyloid fibril formation.[19] Recently, Eakin *et al.*[64] reported a study of $Cu^{2+}$-induced oligomer formation of ß2m under physiological pH. Consistent with our observation,

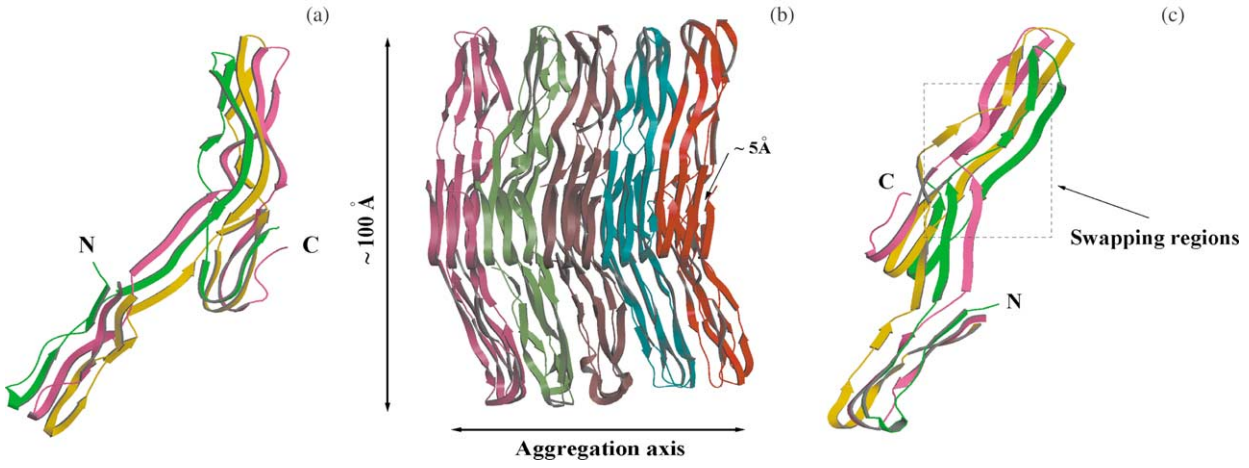


**Figure 4.** (a) A trimer formed by the reduced ß2m. The trimer structure represents a typical snapshot from DMD simulation trajectories near $T_f$. Three monomers in a trimer are represented using yellow, pink and green colors. (b) The model of the reduced ß2m aggregate. We built the aggregate model by using DMD-aided docking (Materials and Methods). Each constituent trimer in the model is represented by a distinct color. The aggregate model is presented with the C-terminal segments of constituent monomers in the front. The width of the aggregate is ~10 nm. The inter-β-sheet distance along the aggregation axis is ~5 Å. (c) Typical structural defects in the trimer structure formed by locally swapping and twisting the global parallel structure.

their study suggests that oxidized ß2m form dimer, tetramer, and other higher-order oligomers by domain-swapping, based on the data from $^{1}$H NMR, near-UV circular dichroism, and analytical ultracentrifugation experiments. Hence, the propagation of domain swapping is the plausible mechanism through which the oxidized ß2m monomers form oligomers.

### Thermodynamic stabilities of the reduced and oxidized ß2m dimers

To analyze the relative thermodynamic stability between monomers and dimers, we first reconstruct all-atom models based on the coarse-grained models from DMD simulations. We then calculate the free energies of both dimers and monomers by the molecular mechanics-Poisson Boltzmann/surface area (MM-PB/SA) method[65] from the trajectories of molecular mechanics simulations. We find that the monomeric oxidized ß2m is more stable than the reduced form by 121.3($\pm$48.0) kcal/mol, which is consistent with DMD simulations and experimental results. The free energy difference between dimeric and monomeric states is $\Delta G = G_{\mathrm{dimer}} - 2G_{\mathrm{monomer}}$, where $G_{\mathrm{dimer}}$ and $G_{\mathrm{monomer}}$ are the free energies of dimer and monomer, respectively. We find that dimers formed by reduced and oxidized ß2m are both less stable than corresponding monomers. The free energy difference between the reduced dimer and two monomers is 540.9($\pm$71.3) kcal/mol. The free energy difference between the oxidized dimer and two monomers is 406.9 ($\pm$71.4) kcal/mol. We note that free energy calculations in molecular mechanics simulations are a challenging task. Hence, we use the values of free energies only for comparison of the relative stabilities between oxidized and reduced forms of dimeric ß2m.

## Discussion

### Distinct aggregation mechanisms of the oxidized and reduced ß2m

We find that the oxidized and reduced ß2m oligomers are formed through distinct mechanisms. Oxidized ß2m forms oligomers by propagation of domain swapping, whereas reduced ß2m forms oligomers by a "parallel stacking" mechanism: extended monomers form inter-chain ß-sheet structure by stacking to each other in a parallel fashion (Figure 5). The domain swapping and parallel stacking mechanisms have different origins. The domain swapping occurs mainly due to competition between native interactions within and between like proteins. Under conditions favoring domain swapping, the fluctuation of unstable structural elements increases and these elements tend to break apart from the rest of the protein and pack onto the complementary parts of other proteins. Thus, a perturbation of these unstable structural elements can have larger effects on promoting fibril formation than others. Jones *et al*.[19] showed that point mutations truncating buried hydrophobic side-chains on N-terminal and C-terminal strands of oxidized ß2m promote rapid fibril formation at neutral pH even in unseeded reactions and increase the rate of fibiril formation at neutral pH. In contrast, similar mutations in the remaining ß-strands of the native protein have little effect on the rate or pH dependence of fibril formation.[19] The domain-swapped structure observed in our simulations is consistent with these results, showing that the N-terminal segments are the exchanging domains. This observation suggests that the local conformational dynamics of N-terminal segment is important for fibrillogenesis onset of ß2m.

The parallel stacking of reduced ß2m results from the competitions of native interactions and non-specific backbone hydrogen-bonding interactions within and between like proteins. Non-specific backbone hydrogen-bonding interactions have been suggested to contribute significantly to amyloidogenesis.[39,66] For example, Guo *et al*. showed that it is possible to form a two-dimensional ß-sheet cooperatively with only backbone hydrogen-bonding.[66] In the native state of the protein, the hydrogen bonds between ß-strands stabilize the sheet structure and the number of dangling hydrogen bonds is minimized.[43,67] When the protein is in a partially folded state, many of the hydrogen bonds within proteins are disrupted. The presence of a large number of unsatisfied hydrogen bonds promotes intermolecular association by forming an intermolecular hydrogen-bonding network. However, the backbone hydrogen bonding may be not the sole factor contributing to the formation of the intermolecular parallel ß-sheets observed in our simulations.

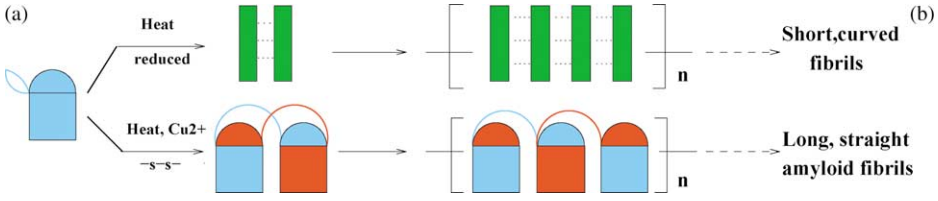


**Figure 5.** Two scenarios of the aggregation. (a) The oxidized ß2m scenario is the propagation of ß2m domain swapping. (b) The reduced ß2m scenario is the parallel stacking of the misfolded ß2m. Semicircles and broken squares represent the N-terminal segment and rest of the native state of ß2m, respectively. The dotted lines between reduced ß2m monomers represent hydrogen bonds.

Specific interactions between like parts of proteins are also important for bringing the partially unfolded monomers close to each other and establishing parallel orientations between them. When a monomer interacts with oligomers, it tends to adopt a similar extended structure to the monomer structure in oligomers, so that the number of backbone hydrogen bond formations is maximized. Thus, a pre-formed oligomer seeds further aggregation by propagation of a hydrogen-bonding network along the aggregation axis.

Both the reduced and oxidized dimers are less stable compared to their corresponding monomers, suggesting that that ß2m oligomerization is not accompanied by the formation of a thermodynamically stable dimer. Interestingly, in a parallel study of Aß oligomerization, Urbanc *et al*.[40] also found that all ten different planar ß-strand dimers formed by Aß peptides have larger free energies with respect to their corresponding monomeric states. These observations suggest that kinetics may play an important role in structure formations of early aggregates.[41]

In spite of the overall structural similarity between dimer and trimer formed by reduced ß2m, there is a difference in structural details. There are more structural irregularities ("defects") in a trimer than in a dimer, whereby they tend to form locally, swapping and twisting the globally parallel structure (Figure 4(c)). These defects, when accumulated within aggregates, disrupt regular organization of the hydrogen-bonding network along the aggregation axis, and ultimately prohibit further formation of fibrils with regular linear geometry. We hypothesize that reduced ß2m are prone to form more defects than the oxidized ß2m upon oligomerization, and, therefore, the reduced ß2m form more flexible filaments than the oxidized ß2m. In addition, the presence of the defects may lead to the curvilinear morphology of the fibrils due to the angular dependence of hydrogen-bonding interactions. Oligomers that are formed without defects grow linearly along the aggregation axis. Oligomers that are formed with defects tend to curve, because defects force favorable hydrogen bonding between monomers to deviate from being parallel to the aggregation axis.

### The role of the disulfide bond

Several studies indicate that the change of disulfide bond formation can result in protein aggregation. It is established that improper disulfide bond formation, concomitant with oxidization, is a main cause of heat-denatured aggregation of T4 lysozyme.[68] It is also proposed that improper disulfide bond formation between intra-molecular free cysteine residues is a mechanism for trapping monomeric SOD1 to the aggregation-prone state.[69] In both cases, structural rearrangement of protein leading to aggregation is directly caused by improper disulfide bond formed either between or within proteins. Along with the improper formation of the disulfide bond, the loss of the disulfide bond is another mechanism to promote the formation of amyloid fibrils *in vitro*.[70,71]

The loss of the disulfide bond does not necessarily cause a direct conformational change in a protein. Instead, such loss may both destabilize the native state and enhance the conformational flexibility of a protein, so that a protein will sample partially folded aggregation-prone states more often. For ß2m, both experiments and our simulations indicate that reducing the disulfide bond results in the destabilization of its native state. The destabilization of the native state has also been shown to be a crucial feature in amyloidosis of transthyretin,[72] immunoglobulin light chains,[73,74] lysozyme,[75] SH3 domains,[39,76] and acylphophatase.[77] However, the destabilization of native state ß2m is not sufficient for the formation of amyloid fibril *in vitro*. It is found that the reduced ß2m monomers are prone to oligomerization but do not form any fibril-like structures when incubated for up to 8 M concentration at pH 7.0 in 0.4 M NaCl.[26] At low pH, the reduced ß2m can only form thinner and flexible fibrous structures that are presumably dead-end products of aggregation.[27] It is other factors such as accumulation of structural defects in the course of the reduced ß2m aggregation that prohibit the formation of typical amyloid fibrils.

The loss of disulfide bond in ß2m also increases the ß2m conformational flexibility, which results in significant loss of its native topology upon oligomerization. In contrast, monomers in domain-swapped dimers formed by oxidized ß2m keep native-like topology. The global native-like topology is also one of the key features shared by several other structural models of oxidized ß2m aggregates, even though the structural details of the models vary.[64,78,79] We postulate that the intact disulfide bond reduces large conformational fluctuations, thereby maintaining the global native-like topology and only allowing local fluctuation of unstable structural elements.

## Conclusions

The hierarchical assembly of amyloid fibrils begins with the formation of oligomers. Unique structures and forming mechanisms of these oligomers define the later pathways of aggregation and final morphology of aggregates. Therefore, the knowledge of the oligomerization process and structural characterization of the precusor oligomeric intermediates is central to understanding the mechanism of fibril assembly and toxicity in amyloid diseases, as well as developing proper therapeutic strategies to inhibit the amyloidogenesis in early stages.[31,34,35] Our study suggests that different aggregation pathways of oxidized and reduced ß2m are dictated by distinct structures and forming mechanisms of precursor oligomeric species (Figure 5), and are modulated by

the disulfide bond. Although environmental variations, such as different pH, ionic strength, and additions of $Cu^{2+}$ affect the precursor oligomeric states and protein aggregation pathways, it is striking that a single disulfide bond modulates ß2m aggregation.

## Materials and Methods

### Protein and interaction model

We perform DMD[47] simulations using a simplified four-bead protein model,[80] in which each residue is represented by three backbone beads N, C, $C^{\alpha}$ and one side-chain bead $C^{\beta}$ (only $C^{\alpha}$ for Gly). The detailed implementation of covalent bonds and constraints that maintain the correct geometry of each residue in the model can be found.[80] In addition to the covalent bonds and constraints, we use the Gō potential[53,54] to model the non-bonded interactions within monomers. The non-bonded interactions between amino acids are only assigned between $C^{\beta}$ atoms ($C^{\alpha}$ for Gly) of corresponding residues:

$$V_{ij} = \begin{cases} +\infty, & |r_i - r_j| \le a \\ \gamma, & a < |r_i - r_j| < b \\ 0, & |r_i - r_j| > b \end{cases} \quad (1)$$

where $|r_i - r_j|$ is the distance between $C^{\beta}$ atoms ($C^{\alpha}$ for Gly) of residues $i$ and $j$ ($i \neq j$). The parameters $a$ and $b$ are the hard-core diameter (3.25 Å) and the cut-off distance (7.5 Å). An attractive potential ($\gamma = -1$) is assigned to all pairs of residues $i$ and $j$ ($i \neq j$) whose $C^{\beta}$ atoms ($C^{\alpha}$ for Gly) are less than 7.5 Å in the native state. A repulsive potential is assigned for the interaction between those whose $C^{\beta}$ atoms ($C^{\alpha}$ for Gly) are separated by more than 7.5 Å in the native state. The ß2m crystal structure (Protein Data Bank accession code 1LDS) is used as native structure to assign the Gō potential. To model the interactions between proteins, we apply the Gō potential between different proteins by assuming that two amino acid residues that attract to each other in a single protein will also have attraction in different proteins.[39] We also incorporate non-specific-backbone hydrogen bonding interaction into the simulations, the detailed implementation of which is described.[80] The strength of the hydrogen bond is $-3$. The disulfide bond interaction between Cys25 and Cys80 is effectively modeled as a covalent bond between $C^{\beta}$ atoms by restraining their distance within the interval from 3.7 Å to 4.2 Å.

### DMD-aided docking

The large protein conformational space makes it impossible to assemble a model of an early aggregate from a random configuration followed by random search strategy. Instead, we position five trimers to form a 15-mer in the parallel stacking scenario to build a structural model of an early aggregate. We use DMD simulations to search for energetically favorable states in the conformational space near a pre-formed configuration of an early aggregate that is consistent with the parallel stacking scenario. The simulation is guided by the following energy function: to keep the overall structure of the ß2m trimers, while allowing backbone flexibility upon docking, we assign the Gō potential of interactions between amino acids based on the starting trimer structure. Hydrogen bonds and inter-molecular interactions are assigned as described in the above oligermization study. Starting from the configuration, in which five trimers are positioned in parallel to each other and separated by 20 Å from each other, a $\sim 10^3$ time units DMD simulation is performed at $T = 0.1$ until the system reaches equilibrium.

### All-atom structure construction and free energy calculation by MM-PB/SA method

We reconstruct all-atom structures of ß2m oligomers by first adding side-chains to coarse-grained models of dimers. We then determine the optimal rotamer states of side-chains by a Monte-Carlo minimization procedure (F. Ding & N.V.D., unpublished results). We further perform molecular dynamics simulations of the reconstructed all-atom models in the explicit solvent using AMBER 8 package.[81] The counter ions of $Na^{+}$ are added to neutralize the system accordingly. Prior to productive simulations, we perform six rounds of energy minimization. First, two consecutive 1000 step energy minimizations are performed with the harmonically constrained protein with spring constants 500 kcal/(mol* Å$^2$) and 250 kcal/(mol* Å$^2$), respectively. Second, two consecutive 1000 step energy minimizations are performed with harmonically constrained water molecules with spring constants 300 kcal/(mol* Å$^2$) and 150 kcal/(mol* Å$^2$) respectively. Third, a 1000-step energy minimization is performed with a harmonically constrained protein with a spring constant 100 kcal/(mol* Å$^2$). Fourth, a 1000 step energy minimization is performed with harmonically constrained water molecules with a spring constant 50 kcal/(mol* Å$^2$). Fifth, a 2500 step energy minimization is performed with the harmonically constrained protein with a spring constant of 10 kcal/(mol* Å$^2$). Last, a 2500 step energy minimization is performed on the whole system without restraints. Prior to the 1000 ps production simulation, 100 ps MD simulation from initial temperature 0 K to 300 K and 1000 ps equilibration simulations at temperature 300 K were performed. The bond length was maintained fixed by the SHAKE algorithm[82] and constant temperature maintained by the weak-coupling algorithm.[83] The trajectories from the 1000 ps production simulations were then used to calculate the free energy of a given molecule by the MM-PB/SA method.[65] The calculation was performed using the AMBER 8 package[84] and the FAMBE program.[85–87]

## Acknowledgements

We thank Dr Feng Ding for suggestions on DMD simulations and manuscript. We also thank Sagar D. Khare for help on using the FAMBE program and Kyle Wilcox for suggestions on the manuscript. This work is supported in part by a Muscular Dystrophy Association grant MDA3720, research grant number 5-FY03-155 from the March of Dimes Birth Defect Foundation, and the UNC/IBM Junior Investigator Award.

## References


1. Gillmore, J. D., Hawkins, P. N. & Pepys, M. B. (1997). Amyloidosis: a review of recent diagnostic and therapeutic developments. *Br. J. Haematol.* **99**, 245–256.
2. Rochet, J. C. & Lansbury, P. T. (2000). Amyloid fibrillogenesis: themes and variations. *Curr. Opin. Struct. Biol.* **10**, 60–68.
3. Dobson, C. M. (1999). Protein misfolding, evolution and disease. *Trends Biochem. Sci.* **24**, 329–332.
4. Jimenez, J. L., Guijarro, J. L., Orlova, E., Zurdo, J., Dobson, C. M., Sunde, M. & Saibil, H. R. (1999). Cryo-electron microscopy structure of an SH3 amyloid fibril and model of the molecular packing. *EMBO J.* **18**, 815–821.
5. Sunde, M. & Blake, C. (1997). The structure of amyloid fibrils by electron microscopy and X-ray diffraction. *Advan. Protein Chem.* **50**, 123–159.
6. Sunde, M., Serpell, L. C., Bartlam, M., Fraser, P. E., Pepys, M. B. & Blake, C. C. (1997). Common core structure of amyloid fibrils by synchrotron X-ray diffraction. *J. Mol. Biol.* **273**, 729–739.
7. Ross, C. A. & Poirier, M. A. (2004). Protein aggregation and neurodegenerative disease. *Nature Med.* **10**, S10–S17.
8. Teplow, D. B. (1998). Structural and kinetic features of amyloid beta-protein fibrillogenesis. *Amyloid*, **5**, 121–142.
9. Prusiner, S. B. (1998). Prions. *Proc. Natl Acad. Sci. USA*, **95**, 13363–13383.
10. Gejyo, F., Yamada, T., Odani, S., Nakagawa, Y., Arakawa, M., Kunitomo, T. *et al*. (1985). A new form of amyloid protein associated with chronic-hemodialysis was identified as beta-2-microglobulin. *Biochem. Biophys. Res. Commun.* **129**, 701–706.
11. Floege, J. & Ketteler, M. (2001). Beta(2)-microglobulin-derived amyloidosis: an update. *Kidney Int.* **59**, S164–S171.
12. Homma, N., Gejyo, F., Isemura, M. & Arakawa, M. (1989). Collagen-binding affinity of beta-2-microglobulin, a preprotein of hemodialysis-associated amyloidosis. *Nephron*, **53**, 37–40.
13. Gejyo, F., Homma, N., Suzuki, Y. & Arakawa, M. (1986). Serum levels of beta 2-microglobulin as a new form of amyloid protein in patients undergoing long-term hemodialysis. *New Engl. J. Med.* **314**, 585–586.
14. Saper, M. A., Bjorkman, P. J. & Wiley, D. C. (1991). Refined structure of the human histocompatibility antigen HLA-A2 at 2.6 Å resolution. *J. Mol. Biol.* **219**, 277–319.
15. Trinh, C. H., Smith, D. P., Kalverda, A. P., Phillips, S. E. & Radford, S. E. (2002). Crystal structure of monomeric human beta-2-microglobulin reveals clues to its amyloidogenic properties. *Proc. Natl Acad. Sci. USA*, **99**, 9771–9776.
16. Isenman, D. E., Painter, R. H. & Dorrington, K. J. (1975). The structure and function of immunoglobulin domains: studies with beta-2-microglobulin on the role of the intrachain disulfide bond. *Proc. Natl Acad. Sci. USA*, **72**, 548–552.
17. Isenman, D. E., Dorrington, K. J. & Painter, R. H. (1975). The structure and function of immunoglobulin domains. II. The importance of interchain disulfide bonds and the possible role of molecular flexibility in the interaction between immunoglobulin G and complement. *J. Immunol.* **114**, 1726–1729.
18. Esposito, G., Michelutti, R., Verdone, G., Viglino, P., Hernandez, H., Robinson, C. V. *et al*. (2000). Removal of the N-terminal hexapeptide from human beta2-microglobulin facilitates protein aggregation and fibril formation. *Protein Sci.* **9**, 831–845.
19. Jones, S., Smith, D. P. & Radford, S. E. (2003). Role of the N and C-terminal strands of beta 2-microglobulin in amyloid formation at neutral pH. *J. Mol. Biol.* **330**, 935–941.
20. Morgan, C. J., Gelfand, M., Atreya, C. & Miranker, A. D. (2001). Kidney dialysis-associated amyloidosis: a molecular role for copper in fiber formation. *J. Mol. Biol.* **309**, 339–345.
21. Chiti, F., De Lorenzi, E., Grossi, S., Mangione, P., Giorgetti, S., Caccialanza, G. *et al*. (2001). A partially structured species of beta 2-microglobulin is significantly populated under physiological conditions and involved in fibrillogenesis. *J. Biol. Chem.* **276**, 46714–46721.
22. Connors, L. H., Shirahama, T., Skinner, M., Fenves, A. & Cohen, A. S. (1985). *In vitro* formation of amyloid fibrils from intact beta 2-microglobulin. *Biochem. Biophys. Res. Commun.* **131**, 1063–1068.
23. Hong, D. P., Gozu, M., Hasegawa, K., Naiki, H. & Goto, Y. (2002). Conformation of beta 2-microglobulin amyloid fibrils analyzed by reduction of the disulfide bond. *J. Biol. Chem.* **277**, 21554–21560.
24. Kad, N. M., Thomson, N. H., Smith, D. P., Smith, D. A. & Radford, S. E. (2001). Beta(2)-microglobulin and its deamidated variant, N17D form amyloid fibrils with a range of morphologies *in vitro*. *J. Mol. Biol.* **313**, 559–571.
25. McParland, V. J., Kad, N. M., Kalverda, A. P., Brown, A., Kirwin-Jones, P., Hunter, M. G. *et al*. (2000). Partially unfolded states of beta(2)-microglobulin and amyloid formation *in vitro*. *Biochemistry*, **39**, 8735–8746.
26. Smith, D. P. & Radford, S. E. (2001). Role of the single disulphide bond of beta(2)-microglobulin in amyloidosis *in vitro*. *Protein Sci.* **10**, 1775–1784.
27. Katou, H., Kanno, T., Hoshino, M., Hagihara, Y., Tanaka, H., Kawai, T. *et al*. (2002). The role of disulfide bond in the amyloidogenic state of beta(2)-microglobulin studied by heteronuclear NMR. *Protein Sci.* **11**, 2218–2229.
28. Ohhashi, Y., Hagihara, Y., Kozhukh, G., Hoshino, M., Hasegawa, K., Yamaguchi, I. *et al*. (2002). The intrachain disulfide bond of beta(2)-microglobulin is not essential for the immunoglobulin fold at neutral pH, but is essential for amyloid fibril formation at acidic pH. *J. Biochem. (Tokyo)*, **131**, 45–52.
29. Bitan, G., Lomakin, A. & Teplow, D. B. (2001). Amyloid beta-protein oligomerization: prenucleation interactions revealed by photo-induced cross-linking of unmodified proteins. *J. Biol. Chem.* **276**, 35176–35184.
30. Bitan, G., Kirkitadze, M. D., Lomakin, A., Vollers, S. S., Benedek, G. B. & Teplow, D. B. (2003). Amyloid beta-protein (Abeta) assembly: Abeta 40 and Abeta 42 oligomerize through distinct pathways. *Proc. Natl Acad. Sci. USA*, **100**, 330–335.
31. Caughey, B. & Lansbury, P. T. (2003). Protofibrils, pores, fibrils, and neurodegeneration: separating the responsible protein aggregates from the innocent bystanders. *Annu. Rev. Neurosci.* **26**, 267–298.
32. Friedhoff, P., von Bergen, M., Mandelkow, E. M., Davies, P. & Mandelkow, E. (1998). A nucleated assembly mechanism of Alzheimer paired helical filaments. *Proc. Natl Acad. Sci. USA*, **95**, 15712–15717.
33. Kayed, R., Bernhagen, J., Greenfield, N., Sweimeh, K., Brunner, H., Voelter, W. & Kapurniotu, A. (1999).

Conformational transitions of islet amyloid polypeptide (IAPP) in amyloid formation *in vitro*. *J. Mol. Biol.* **287**, 781–796.
34. Kelly, J. W. (1998). The alternative conformations of amyloidogenic proteins and their multi-step assembly pathways. *Curr. Opin. Struct. Biol.* **8**, 101–106.
35. Kirkitadze, M. D., Bitan, G. & Teplow, D. B. (2002). Paradigm shifts in Alzheimer's disease and other neuro degenerative disorders: the emerging role of oligomeric assemblies. *J. Neurosci. Res.* **69**, 567–577.
36. Harper, J. D. & Lansbury, P. T., Jr (1997). Models of amyloid seeding in Alzheimer's disease and scrapie: mechanistic truths and physiological consequences of the time-dependent solubility of amyloid proteins. *Annu. Rev. Biochem.* **66**, 385–407.
37. Lansbury, P. T., Jr (1997). Inhibition of amyloid formation: a strategy to delay the onset of Alzheimer's disease. *Curr. Opin. Chem. Biol.* **1**, 260–267.
38. Scherzinger, E., Sittler, A., Schweiger, K., Heiser, V., Lurz, R., Hasenbank, R. *et al*. (1999). Self-assembly of polyglutamine-containing huntingtin fragments into amyloid-like fibrils: implications for Huntington's disease pathology. *Proc. Natl Acad. Sci. USA*, **96**, 4604–4609.
39. Ding, F., Dokholyan, N. V., Buldyrev, S. V., Stanley, H. E. & Shakhnovich, E. I. (2002). Molecular dynamics simulation of the SH3 domain aggregation suggests a generic amyloidogenesis mechanism. *J. Mol. Biol.* **324**, 851–857.
40. Urbanc, B., Cruz, L., Ding, F., Sammond, D., Khare, S., Buldyrev, S. V. *et al*. (2004). Molecular dynamics simulation of amyloid beta dimer formation. *Biophys. J.* **87**, 2310–2321.
41. Hwang, W., Zhang, S., Kamm, R. D. & Karplus, M. (2004). Kinetic control of dimer structure formation in amyloid fibrillogenesis. *Proc. Natl Acad. Sci. USA*, **101**, 12916–12921.
42. Smith, A. V. & Hall, C. K. (2001). Protein refolding *versus* aggregation: computer simulations on an intermediate-resolution protein model. *J. Mol. Biol.* **312**, 187–202.
43. Thirumalai, D., Klimov, D. K. & Dima, R. I. (2003). Emerging ideas on the molecular basis of protein and peptide aggregation. *Curr. Opin. Struct. Biol.* **13**, 146–159.
44. DeMarco, M. L. & Daggett, V. (2004). From conversion to aggregation: protofibril formation of the prion protein. *Proc. Natl Acad. Sci. USA*, **101**, 2293–2298.
45. Dima, R. I. & Thirumalai, D. (2004). Probing the instabilities in the dynamics of helical fragments from mouse PrPc. *Proc. Natl Acad. Sci. USA*, **101**, 15335–15340.
46. Ma, B. & Nussinov, R. (2003). Molecular dynamics simulations of the unfolding of beta(2)-microglobulin and its variants. *Protein Eng.* **16**, 561–575.
47. Rapaport, D. C. (1997). *The Art of Molecular Dynamics Simulation*, Cambridge University Press, Cambridge.
48. Borreguero, J. M., Dokholyan, N. V., Buldyrev, S. V., Shakhnovich, E. I. & Stanley, H. E. (2002). Thermodynamics and folding kinetics analysis of the SH3 domain form discrete molecular dynamics. *J. Mol. Biol.* **318**, 863–876.
49. Zhou, Y. & Karplus, M. (1999). Folding of a model three-helix bundle protein: a thermodynamic and kinetic analysis. *J. Mol. Biol.* **293**, 917–951.
50. Dokholyan, N. V., Buldyrev, S. V., Stanley, H. E. & Shakhnovich, E. I. (1998). Discrete molecular dynamics studies of the folding of a protein-like model. *Fold. Des.* **3**, 577–587.
51. Smith, A. V. & Hall, C. K. (2001). Alpha-helix formation: discontinuous molecular dynamics on an intermediate-resolution protein model. *Proteins: Struct. Funct. Genet.* **44**, 344–360.
52. Smith, S. W., Hall, C. K. & Freeman, B. D. (1997). Molecular dynamics for polymeric fluids using discontinuous potentials. *J. Comput. Phys.* **134**, 16–30.
53. Abe, H. & Go, N. (1981). Non-interacting local-structure model of folding and unfolding transition in globular-proteins. 2. Application to two-dimensional lattice proteins. *Biopolymers*, **20**, 1013–1031.
54. Go, N. & Abe, H. (1981). Non-interacting local-structure model of folding and unfolding transition in globular-proteins. 1. Formulation. *Biopolymers*, **20**, 991–1011.
55. Halverson, K., Fraser, P. E., Kirschner, D. A. & Lansbury, P. T. (1990). Molecular determinants of amyloid deposition in alzheimers-disease—conformational studies of synthetic beta-protein fragments. *Biochemistry*, **29**, 2639–2644.
56. Lansbury, P. T., Jr, Costa, P. R., Griffiths, J. M., Simon, E. J., Auger, M., Halverson, K. J. *et al*. (1995). Structural model for the beta-amyloid fibril based on interstrand alignment of an antiparallel-sheet comprising a C-terminal peptide. *Nature Struct. Biol.* **2**, 990–998.
57. Benzinger, T. L., Gregory, D. M., Burkoth, T. S., Miller-Auer, H., Lynn, D. G., Botto, R. E. & Meredith, S. C. (1998). Propagating structure of Alzheimer's beta-amyloid(10-35) is parallel beta-sheet with residues in exact register. *Proc. Natl Acad. Sci. USA*, **95**, 13407–13412.
58. Liu, Y. & Eisenberg, D. (2002). 3D domain swapping: as domains continue to swap. *Protein Sci.* **11**, 1285–1299.
59. Knaus, K. J., Morillas, M., Swietnicki, W., Malone, M., Surewicz, W. K. & Yee, V. C. (2001). Crystal structure of the human prion protein reveals a mechanism for oligomerization. *Nature Struct. Biol.* **8**, 770–774.
60. Liu, Y., Gotte, G., Libonati, M. & Eisenberg, D. (2001). A domain-swapped RNase A dimer with implications for amyloid formation. *Nature Struct. Biol.* **8**, 211–214.
61. Liu, Y., Gotte, G., Libonati, M. & Eisenberg, D. (2002). Structures of the two 3D domain-swapped RNase A trimers. *Protein Sci.* **11**, 371–380.
62. Green, S. M., Gittis, A. G., Meeker, A. K. & Lattman, E. E. (1995). One-step evolution of a dimer from a monomeric protein. *Nature Struct. Biol.* **2**, 746–751.
63. Staniforth, R. A., Giannini, S., Higgins, L. D., Conroy, M. J., Hounslow, A. M., Jerala, R. *et al*. (2001). Three-dimensional domain swapping in the folded and molten-globule states of cystatins, an amyloid-forming structural superfamily. *EMBO J.* **20**, 4774–4781.
64. Eakin, C. M., Attenello, F. J., Morgan, C. J. & Miranker, A. D. (2004). Oligomeric assembly of native-like precursors precedes amyloid formation by beta-2 microglobulin. *Biochemistry*, **43**, 7808–7815.
65. Lee, M. R., Duan, Y. & Kollman, P. A. (2000). Use of MM-PB/SA in estimating the free energies of proteins: application to native, intermediates, and unfolded villin headpiece. *Proteins: Struct. Funct. Genet.* **39**, 309–316.
66. Guo, C. L., Cheung, M. S., Levine, H. & Kessler, D. A. (2002). Mechanisms of cooperativity underlying sequence-independent beta-sheet formation. *J. Chem. Phys.* **116**, 4353–4365.

67. Richardson, J. S. & Richardson, D. C. (2002). Natural beta-sheet proteins use negative design to avoid edge-to-edge aggregation. *Proc. Natl Acad. Sci. USA*, **99**, 2754–2759.
68. Perry, L. J. & Wetzel, R. (1987). The role of cysteine oxidation in the thermal inactivation of T4 lysozyme. *Protein Eng.* **1**, 101–105.
69. Khare, S. D., Ding, F. & Dokholyan, N. V. (2003). Folding of Cu, Zn superoxide dismutase and familial amyotrophic lateral sclerosis. *J. Mol. Biol.* **334**, 515–525.
70. Klafki, H. W., Pick, A. I., Pardowitz, I., Cole, T., Awni, L. A., Barnikol, H. U. *et al*. (1993). Reduction of disulfide bonds in an amyloidogenic Bence Jones protein leads to formation of "amyloid-like" fibrils *in vitro*. *Biol. Chem. Hoppe Seyler*, **374**, 1117–1122.
71. Swietnicki, W., Morillas, M., Chen, S. G., Gambetti, P. & Surewicz, W. K. (2000). Aggregation and fibrillization of the recombinant human prion protein huPrP90-231. *Biochemistry*, **39**, 424–431.
72. Lai, Z., Colon, W. & Kelly, J. W. (1996). The acid-mediated denaturation pathway of transthyretin yields a conformational intermediate that can self-assemble into amyloid. *Biochemistry*, **35**, 6470–6482.
73. Helms, L. R. & Wetzel, R. (1996). Specificity of abnormal assembly in immunoglobulin light chain deposition disease and amyloidosis. *J. Mol. Biol.* **257**, 77–86.
74. Raffen, R., Dieckman, L. J., Szpunar, M., Wunschl, C., Pokkuluri, P. R., Dave, P. *et al*. (1999). Physicochemical consequences of amino acid variations that contribute to fibril formation by immunoglobulin light chains. *Protein Sci.* **8**, 509–517.
75. Booth, D. R., Sunde, M., Bellotti, V., Robinson, C. V., Hutchinson, W. L., Fraser, P. E. *et al*. (1997). Instability, unfolding and aggregation of human lysozyme variants underlying amyloid fibrillogenesis. *Nature*, **385**, 787–793.
76. Guijarro, J. I., Sunde, M., Jones, J. A., Campbell, I. D. & Dobson, C. M. (1998). Amyloid fibril formation by an SH3 domain. *Proc. Natl Acad. Sci. USA*, **95**, 4224–4228.
77. Chiti, F., Webster, P., Taddei, N., Clark, A., Stefani, M., Ramponi, G. & Dobson, C. M. (1999). Designing conditions for *in vitro* formation of amyloid protofilaments and fibrils. *Proc. Natl Acad. Sci. USA*, **96**, 3590–3594.
78. Benyamini, H., Gunasekaran, K., Wolfson, H. & Nussinov, R. (2003). beta(2)-microglobulin amyloidosis: insights from conservation analysis and fibril modelling by protein docking techniques. *J. Mol. Biol.* **330**, 159–174.
79. Ivanova, M. I., Sawaya, M. R., Gingery, M., Attinger, A. & Eisenberg, D. (2004). An amyloid-forming segment of beta2-microglobulin suggests a molecular model for the fibril. *Proc. Natl Acad. Sci. USA*, **101**, 10584–10589.
80. Ding, F., Borreguero, J. M., Buldyrey, S. V., Stanley, H. E. & Dokholyan, N. V. (2003). Mechanism for the alpha-helix to beta-hairpin transition. *Proteins: Struct. Funct. Genet.* **53**, 220–228.
81. Pearlman, D. A., Case, D. A., Caldwell, J. W., Ross, W. S., Cheatham, T. E., Debolt, S. *et al*. (1995). Amber, a package of computer-programs for applying molecular mechanics, normal-mode analysis, molecular-dynamics and free-energy calculations to simulate the structural and energetic properties of molecules. *Comput. Phys. Commun.* **91**, 1–41.
82. Ryckaert, J. P., Ciccotti, G. & Berendsen, H. J. C. (1977). Numerical integration of the cartesian equations of motion of a system with constraints: molecular dynamics of *n*-alkanes. *J. Comput. Phys.* **23**, 327–341.
83. Berendsen, H. J. C., Postma, J. P. M., Vangunsteren, W. F., Dinola, A. & Haak, J. R. (1984). Molecular-dynamics with coupling to an external bath. *J. Chem. Phys.* **81**, 3684–3690.
84. Pearlman, D. A., Case, D. A., Caldwell, J. W., Ross, W. S., Cheatham, T. E., Debolt, S. *et al*. (1995). Amber, a package of computer-programs for applying molecular mechanics, normal-mode analysis, molecular-dynamics and free-energy calculations to simulate the structural and energetic properties of molecules. *Comput. Phys. Commun.* **91**, 1–41.
85. Vorobjev, Y. N. & Scheraga, H. A. (1997). A fast adaptive multigrid boundary element method for macromolecular electrostatic computations in a solvent. *J. Comput. Chem.* **18**, 569–583.
86. Vorobjev, Y. N. & Hermans, J. (1997). SIMS: computation of a smooth invariant molecular surface. *Biophys. J.* **73**, 722–732.
87. Vorobjev, Y. N., Almagro, J. C. & Hermans, J. (1998). Discrimination between native and intentionally misfolded conformations of proteins: ES/IS, a new method for calculating conformational free energy that uses both dynamics simulations with an explicit solvent and an implicit solvent continuum model. *Proteins: Struct. Funct. Genet.* **32**, 399–413.
88. Kraulis, P. J. (1991). Molscript—a program to produce both detailed and schematic plots of protein structures. *J. Appl. Crystallog.* **24**, 946–950.
89. Merritt, E. A. & Bacon, D. J. (1997). Raster3D: photorealistic molecular graphics. *Macromol. Crystallog.* **277**, 505–524.

***Edited by P. T. Lansbury Jr***

*(Received 19 May 2005; received in revised form 24 August 2005; accepted 25 September 2005)*
Available online 7 October 2005